Published OnlineFirst June 15, 2017; DOI: 10.1158/0008-5472.CAN-16-2501

Microenvironment and Immunology

Cancer Research

Heme-oxygenase-1 Production by Intestinal CX3CR1^{+} Macrophages Helps to Resolve Inflammation and Prevents Carcinogenesis

Giulia Marelli[1], Marco Erreni[1], Achille Anselmo[1], Valentina Taverniti[2], Simone Guglielmetti[2], Alberto Mantovani[1,3], and Paola Allavena[1,3]

Abstract

CX3CR1^{+} macrophages in the intestinal lamina propria contribute to gut homeostasis through the immunomodulatory interleukin IL10, but there is little knowledge on how these cells or the CX3CR1 receptor may affect colorectal carcinogenesis. In this study, we show that CX3CR1-deficient mice fail to resolve gut inflammation despite high production of IL10 and have increased colitis and adenomatous polyps in chemical and genetic models of colon carcinogenesis. Mechanistically, CX3CL1-mediated engagement of the CX3CR1 receptor induced upregulation of heme-oxygenase-1 (HMOX-1), an antioxidant and anti-inflammatory enzyme. CX3CR1-deficient mice exhibited significantly lower expression of HMOX-1 in their adenomatous colon tissues. Combining LPS and CX3CL1 displayed a strong synergistic effect *in vitro*, but HMOX-1 levels were significantly lower in KO macrophages. Cohousing of wild-type and CX3CR1$^{-/-}$ mice during the AOM/DSS treatment attenuated disease severity in CX3CR1$^{-/-}$ mice, indicating the importance of the microbiome, but did not fully reinstate HMOX-1 levels and did not abolish polyp formation. In contrast, pharmacologic induction of HMOX-1 *in vivo* by cobalt protoporphyrin-IX treatment eradicated intestinal inflammation and fully protected KO mice from carcinogenesis. Taken together, our results establish an essential role for the receptor CX3CR1 in gut macrophages in resolving inflammation in the intestine, where it helps protects against colitis-associated cancer by regulating HMOX-1 expression. *Cancer Res; 77(16); 4472–85. ©2017 AACR.*

Introduction

Gut represents a complex landscape in which commensal bacteria, harmless antigens, and food proteins are strictly in contact with the immune system that has to be able to maintain a balance between the immune response and tolerance (1–3). If this crucial checkpoint is lost, the immune system is activated and falls in a dangerous and prolonged inflammation (4). In this context, mononuclear phagocytes are the most abundant population and among them macrophages characterized by the expression of the chemokine receptor CX3CR1 represent key players in this process of discrimination, by allowing a peaceful coexistence. Mucosal CX3CR1^{+} cells are nowadays considered a population of resident macrophages in the gut, continuously replenished from blood stream monocytes (5–7). Fractalkine (FKN-CX3CL1) is the only ligand of the chemokine receptor CX3CR1 (8) and, although it has been reported to be involved in the attraction of monocytes/macrophages in several tissues, in the gut is not regulating monocyte recruitment. The current knowledge is that CX3CR1^{+} macrophages derive from inflammatory Ly6C^{Hi} CX3CR1^{Neg} monocytes, which are recruited in the intestine via the CCR2–CCL2 axis, where they upregulate the CX3CR1 receptor once they have reached the tissue (6, 9). In healthy conditions, Ly6C^{Hi} monocytes mature into CX3CR1^{Hi} macrophages expressing diverse levels of CX3CR1 during maturation stages. The process of maturation from CX3CR1^{Int} to CX3CR1^{Hi} macrophages is interrupted during colitis, allowing the expansion of proinflammatory CX3CR1^{Int} macrophages that are able to face pathogens (5).

In the gut, CX3CR1^{+} macrophages are able to sample luminal antigens and transfer them to local dendritic cells to initiate or block the immune response (10–15). Furthermore, they produce and sense the anti-inflammatory cytokine IL10 to maintain homeostasis (5, 6, 16, 17).

The role of gut CX3CR1^{+} macrophages has been studied taking advantage of the availability of mice carrying the GFP reporter protein in 1 allele of the CX3CR1 gene (CX3CR1$^{GFP/+}$) or in both alleles (CX3CR1$^{GFP/GFP}$ or KO mice; refs. 5, 18). Few reports have investigated the behavior of mucosal CX3CR1-deficient macrophages during experiments of acute intestinal inflammation induced by chemical injury (Dextran Sodium Sulphate, DSS) or bacterial infections. These studies reported controversial results, with either higher or lower recruitment of inflammatory cells in the intestine, and increased or decreased inflammation (19–22).

Our recent study clearly indicated that CX3CR1 KO mice have more severe acute colitis (23); however, how the CX3CR1 receptor is involved in the molecular mechanisms that

[1]Departement of Immunology and Inflammation, IRCCS-Humanitas Clinical and Research Center, Via Manzoni, Rozzano, Milano, Italy. [2]Department of Food, Environmental and Nutritional Sciences (DeFENS), Division of Food Microbiology and Bioprocesses, Università degli Studi di Milano, Milano, Italy. [3]Humanitas University, Rozzano, Milano, Italy.

Note: Supplementary data for this article are available at Cancer Research Online (http://cancerres.aacrjournals.org/).

Corresponding Authors: Giulia Marelli, Department of Immunology and Inflammation, IRCCS-Humanitas Clinical and Research Center, Via Manzoni, 56, Rozzano, Milano 20089, Italy. Phone: 3932-0023-9969; Fax: 3902-8224-5136; E-mail: giulia.p.marelli@gmail.com; and Paola Allavena, paola.allavena@humanitasresearch.it

doi: 10.1158/0008-5472.CAN-16-2501

Published OnlineFirst June 15, 2017; DOI: 10.1158/0008-5472.CAN-16-2501

regulate the inflammatory response is still unclear. Moreover, no data are available on the role of CX3CR1^{+} macrophages in models of prolonged inflammation, such the colitis-induced carcinogenesis.

In this study, we unveil the role of the CX3CR1 receptor in the homeostatic function of mucosal macrophages. We report that CX3CR1-deficient mice have a more severe disease in models of colon carcinogenesis, with increased inflammation sustained over time. We demonstrate that ligand activation of CX3CR1 induces the production of heme-oxygenase-1 (HMOX-1), a crucial antioxidant and anti-inflammatory enzyme, which decreases inflammation, protects the colonic mucosa, and prevents the development of gut carcinogenesis.

Materials and Methods

Mouse models

Procedures involving animal care conformed to national (4D.L. N.116, G.U. 1992) and international laws (EEC Council Directive 2010/63/EU, OJ L 276/33, 22.09.2010). Mice were maintained in a specific-pathogen free facility. All efforts were made to minimize the number of animals used and their suffering. All experiments were designed using C57BL/6 mice. We compared CX3CR1$^{+/GFP}$ (WT) to CX3CR1$^{GFP/GFP}$ (KO) and CX3CR1$^{+/GFP}$-APC^{min} (WT) to CX3CR1$^{GFP/GFP}$-APC^{min} (KO). Usually 8 mice per group aged 8 weeks were used for each *in vivo* model. Table 1 schematically lists the different treatments. Cobalt protoporphyrin IX (coPP) was prepared in dim light due to its photosensibility and dissolved in sodium hydroxide (NaOH) 150 mmol/L. pH was adjusted to 7 by adding equal amount of hydrochloric acid (HCl) at the final concentration of 5 mg/mL. The final pH of 7.4 was achieved by further dilution with PBS without calcium and magnesium (PBS$^{-/-}$, BioSera).

Histologic analysis

Colons were harvested and longitudinally opened; next, they were rolled up transversely (swiss roll). Tissues were then fixed in 4% paraformaldehyde (PFA) and dehydrated in 30% and 40% sucrose in PBS$^{-/-}$. Next, the colonic tissues were embedded in optimum cutting temperature compound (OCT, Diapath) and stored at −80°C. To evaluate the histologic architecture of the inflamed colon and calculate the percentage of the adenomatous area over the total tissue, 8-μm thick frozen sections were cut with cryostat and stained with hematoxylin and eosin (H&E stain). Slides were observed with microscope (4×) and colitis score was assessed. To define polyps' growth, slides were scanned with VS120 Dotslide (Olympus) and analyzed with OLYVIA software. For immunofluorescence staining, frozen tissue sections (8 μm) were incubated with the primary antibody(ies) in washing buffer (1 hour at room temperature) and subsequently with fluorophore-conjugated secondary antibody(ies) at room temperature for 1 hour in the dark (1:2,000). Finally, cell nuclei counterstained with DAPI. Images were captured with the Olympus FluoViewTM FV1000 confocal microscope. The acquired images were analysed with "(Fiji is just) ImageJ software". Multichannel images were split to the respective components and every channel was transformed into a binary image. According to the "set measure" option, the percentage of stained tissue in each component was calculated overall the total black background of the single slide. Considering the DAPI-stained tissue as the entire tissue (100%), we finally calculated the percentage of tissue stained by every single fluorophore using the mathematical proportion: %DAPI:100 = %fluorophore: X

RNA extraction and quantitative real-time PCR. Total RNA was extracted from colon tissue. In the colitis-associated cancer (CAC) experiments, polyps were separated from the rest of the colon and analyzed independently. Samples were homogenized in TRIzol (Ambion) using Tissue Lyser II (Quiagen). One microgram of RNA was reverse-transcribed using the High Capacity cDNA Reverse Transcription Kit (Applied Biosystems) following manufacturer's instructions. cDNA analyzed through quantitative real-time PCR, performed on Viia-7 instrument (Thermo Fisher) using the Fast SYBR Green. *GAPDH* gene was amplified as internal control. The other primers are listed in Supplemental Materials and Figures.

Western blot analysis. Quantification of HMOX-1 protein was tested in treated colons through SDS-PAGE and Western blotting assay. Samples were harvested after sacrifice and protein extracted using Urea buffer (Urea 9 mol/L, 25 mmol/L Tris-HCl pH 6.8, 1 mmol/L EDTA, 10% glycerol). Twenty-five micrograms of total proteins were resolved on 10% SDS-PAGE and transferred onto Trans Blot Transfer Medium, nitrocellulose membrane (Bio-Rad). After blocking, the membrane was incubated overnight with HMOX-1 antibody. After the incubation with the membranes were developed with chemiluminescence reagent (Bio-Rad), according to the manufacturer's instructions, and visualized with Chemidoc System (Bio-Rad).

Generation of bone marrow–derived macrophages. Bone marrow was harvested from femurs of 8- to 12-week old mice by flushing the marrow out with IMDM supplemented with 10% fetal calf serum (FCS) and ACK (100 μL/bone). Flushed cells were resuspended in 20 mL IMDM, 10% FCS, 1% penicillin/streptavidin, 1% glutammine and let to adhere overnight at 37°C, 5% CO_2. After incubation, cell supernatant was removed, nonadherent cells were spun down. Cells were stained as described and then FACS-sorted using BD FACS Aria and resuspended at the concentration of 0.5×10^6 cells/mL in complete bone marrow macrophage medium (IMDM, 10% FCS, 20 ng/mL M-CSF) in suspension culture dish (Corning; 10 mL/dish). After 7 days, cells were plated at the final concentration of 2.5×10^5 cells/mL in 24 wells plated and stimulated with LPS (100 ng/mL), recombinant Fractalkine (FKN, 300 ng/mL) or LPS-FKN. Cells were lysated to recover RNA as already described, and used for qPCR analysis.

Isolation of mononuclear cells from lamina propria. To isolate lamina propria mononuclear cells (LPMC), colons were then flushed of their luminal content, opened longitudinally and cut into 1-cm pieces. Epithelial cells were removed by 40-minute incubation with HBSS (without Ca2+ and Mg2+) containing 5% FBS, 2 mmol/L EDTA at 37°C, shaking at 275 rpm. Colon pieces were then digested in HBSS$^{-/-}$ containing 5% FBS, 0.5 mg/mL Collagenase VIII (Sigma), for 40 minutes at 37°C shaking at 275 rpm. The obtained cell suspension was then pressed into a syringe needle, washed with RPMI, and passed sequentially through 100- and 40-μm cell strainers. Cells were centrifuged for 6 minutes at 1,600 rpm, resuspended in RPMI, and used for the subsequent analysis.

Flow cytometry. Briefly, cells were harvested from colon samples of both polyps, inflamed colon, and healthy control as described

Published OnlineFirst June 15, 2017; DOI: 10.1158/0008-5472.CAN-16-2501

before. Cells were washed with FACS buffer ($PBS^{-/-}$, 2% FBS), and incubated 30 minutes at 4°C with antibodies and suspended in 350 μL of FACS buffer. Immediately, cells were read using FACSCanto II instrument and FACS Diva software version 6.1.1 (BD Biosciences). For each experiment, cells were stained with appropriate isotype control antibodies to establish background staining before calculating the percentage of positive cells.

Phospho-protein detection. To detect the expression of phosphorylated protein, 2×10^6 cells were suspended in DMEM at 37°C and stimuli were added (IL10 25 ng/mL, FKN 300 ng/mL) to a final volume of 300 μL. Cells were treated for 5, 30, or for 120 minutes. After the treatment, PFA were added to fix the cells. Cold methanol was added for 20 minutes to permeabilize cells and samples were stained with pSTAT3 (py705-BD) for 30 minutes at room temperature in the dark. After the incubation, cells were washed and suspended in 350 μL of FACS buffer ($PBS^{-/-}$, FBS 1%, NaN_3 0.1%) and analyzed with FACS CANTO II instrument.

Phagocytosis assay. Peritoneal-elicited macrophages were harvested from WT and KO mice. Briefly, 1 mL of thioglycolate (3% thioglycolate medium without dextrose, BD Biosciences) was injected intraperitoneally (i.p.). After three days, mice were sacrificed and 10 mL of cold physiologic solution were injected in the peritoneum, cells were collected and kept in ice. Live cells were sorted using FACSAria instrument based on GFP gene reporter expression. After, 2×10^5 cells were plate on glass slides in 24 wells in DMEM overnight. In the meantime, polystyrene latex beads (Sigma-Aldrich), 3 μm in diameter were coated with LPS diluted 1:100 in bicarbonate buffer in a ratio of 1:10 cells/beads by incubating for 1 hour at 37°C shaking. Beads were washed once with $HBSS^{-/-}$ and added to cells for 1 hour. The excess of beads was washed out and cells stained and fixed with DiffQuik (medion diagnostics) and mounted on glass. Beads were counted at the microscope, analyzing ten fields for each samples. The percentage of phagocytosis was calculated as follow: *n* cells: *n* bead = 100: x.

Reagents

The following antibodies were used. Immunofluorescence: rat anti-mouse F4/80 mAb (eBioscience) 1:500, rabbit anti-human Zo-1 (Invitrogen) polyclonal antibody 1:200, rabbit anti-human HMOX-1 polyclonal antibody (Bio-Rad) 1:500. Western blot analysis: rabbit anti-mouse HMOX-1 antibody (ProteinTech) 1:600. Flow cytometry: CD45 percP (BD Biosciences), CD11b pacific blue (eBiolegend), F4/80 PE (Serotec), Ly6G PE-cy7 (BD Biosciences), Ly6C APC (BD Biosciences), pSTAT3 (py705-BD Biosciences).

Microbioma profiling

The bacterial community structure of fecal samples was determined by 16S rRNA gene profiling as described previously (24). In brief, a DNA fragment encompassing the variable region V3 of the 16S rRNA gene was amplified from fecal metagenomic DNA with the primers Probio_Uni (5′-CCTACGGGRSGCAGCAG-3′) and Probio_Rev (5′-ATTACCGCGGCTGCT-3′) and was sequenced by means of Ion Torrent PGM sequencing technology (Life Technologies). Sequence reads were analyzed using the bioinformatic pipeline Quantitative Insights Into Microbial Ecology (QIIME) version 1.7.0 (25) with the GreenGenes database updated to version 13.5. Bacterial relative abundances in fecal sample were studied at the taxonomic levels of phylum, family, and genus. Details are listed in the online Supplementary files.

Statistical analysis

Statistical analysis was performed with GraphPad Prism 6 (GraphPad Software). To compare different datasets, unpaired two-tailed Student *t* test was used and results were expressed as mean ± SEM for the histograms and as median, quartiles, 5th–95th percentiles for the whiskers box. A value of $P < 0.05$ (*) was considered as statistically significant.

Results

The chemically induced colitis-associated cancer is more severe in $CX3CR1^{GFP/GFP}$ mice

We used the model of CAC induced by the carcinogen azoxymethane (AOM) and dextran sulfate sodium (DSS) in mice proficient and deficient for the chemokine receptor CX3CR1 ($CX3CR1^{+/GFP}$ and $CX3CR1^{GFP/GFP}$ mice). AOM was intraperitoneally injected and a week after mice were fed with DSS, followed by water for two weeks, for a total of three cycles, as schematically presented in Fig. 1A. During treatment, mice were monitored for weight, stool consistency, and bleeding, to score Disease Activity Index (DAI). After the first cycle of DSS, both KO and WT mice showed loss in weight and signs of bleeding, but during the recovery phase with water, WT mice gained weight (Supplementary Fig. S1A) and stopped bleeding, while KO mice failed to recover (Fig. 1B). During further cycles, the difference between WT and KO became even stronger, in particular for the inability of KO mice to regain weight. At the end of the experiment, after 70 days, colons were harvested and histologically analyzed. KO mice showed higher colitis scores and reduced colon length (Fig. 1C), indicating they had more severe inflammation compared with WT mice. Consistent with this, KO mice had a significantly higher percentage of adenomatous polyps (Fig. 1C) and lower survival rate (Supplementary Fig. S1B).

Increased macrophage infiltration and cytokine production in the colons of $CX3CR1^{GFP/GFP}$ mice

By immunofluorescence of colon sections, we observed that CX3CR1-KO mice presented a higher number of GFP^{Pos}

Table 1. Experimental procedures in mice

Treatment	Procedure	Sacrifice
Acute colitis	3% DSS in drinking water for 7 days.	Day 7
Recovery from colitis	3% DSS in drinking water for 7 days.	Day 10–13
Colitis-associated cancer	i.p. injection of azoxymethane (10 mg/kg, SIGMA), followed by 3% DSS in drinking water for 6 days, and fresh water for 15 days. DSS treatment was repeated for a total of 3 rounds	Day 70
CoPP injection	i.p. injection of 150 ug of coPP or vehicle (NaOH and HCl) in a final volume of 200 ul, 4 times a week during each cycle of DSS administration (day −1, 0, 3, 6)	Day 70
Carcinogenesis in APC^{Min} mice	2,5% DSS in drinking water for 7 days, followed by fresh water for 28 days.	Day 35

Published OnlineFirst June 15, 2017; DOI: 10.1158/0008-5472.CAN-16-2501

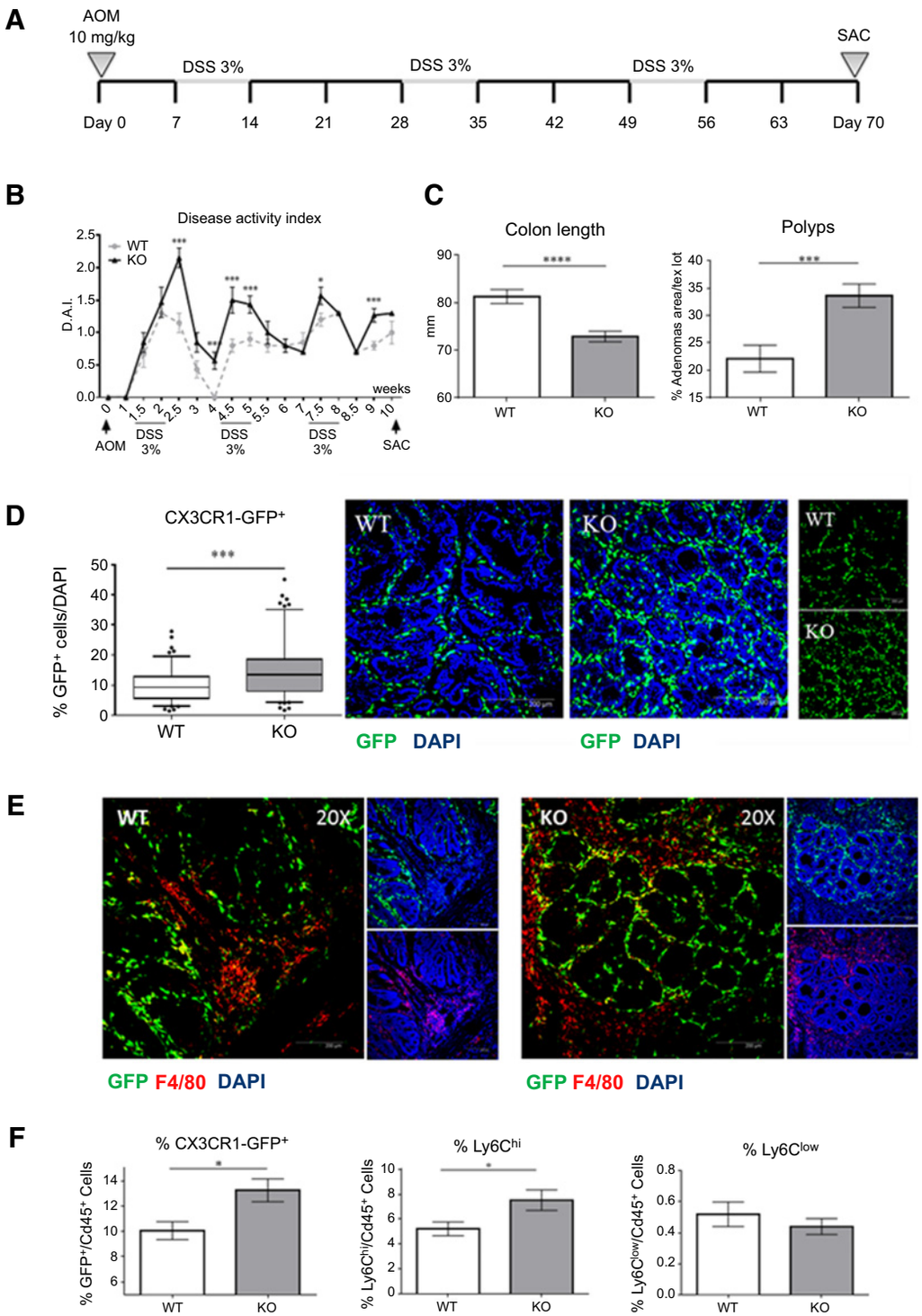

Figure 1.

Colitis-associated carcinogenesis is more severe in CX3CR1$^{GFP/GFP}$ (KO mice). **A,** Treatment scheme of the AOM/DSS protocol in CX3CR1$^{GFP/GFP}$ and CX3CR1$^{+/GFP}$ mice. Disease activity index (as described in Materials and Methods; **B**) and polyps' number are higher in KO mice while colon length is shorter (**C**). **D,** Immunofluorescence of GFP^{+} macrophages in the polyps of CX3CR1$^{GFP/GFP}$ and CX3CR1$^{+/GFP}$ mice after treatment with AOM/DSS; KO mice have increased infiltration of GFP^{+} macrophages. **E,** Immunofluorescence with anti-F4/80 (red); newly recruited macrophages (F4/80^{+} GFP^{neg}) mainly accumulate at the adenomatous border, while resident GFP^{+} macrophages are inside the polyp; several double positive (F4/80^{+} GFP^{pos}) macrophages are also visible (yellow). Magnification, ×20. GFP, green; DAPI, blue. **F,** FACS analysis of disaggregated polyps confirms the higher accumulation of GFP^{+} macrophages and inflammatory LyC6^{hi} monocytes (precursors of CX3CR1^{+} macrophages) in KO mice, while no differences were found for LyC6^{low} myeloid cells. Results in **B** and **F** are from one experiment with 8 mice per group, representative of five experiments performed with similar results. In **C** and **D,** results are the mean ± SEM of five experiments. *t* test; *, $P < 0,05$; **, $P < 0,01$; ***, $P < 0,001$; ****, $P < 0,0001$.

Published OnlineFirst June 15, 2017; DOI: 10.1158/0008-5472.CAN-16-2501

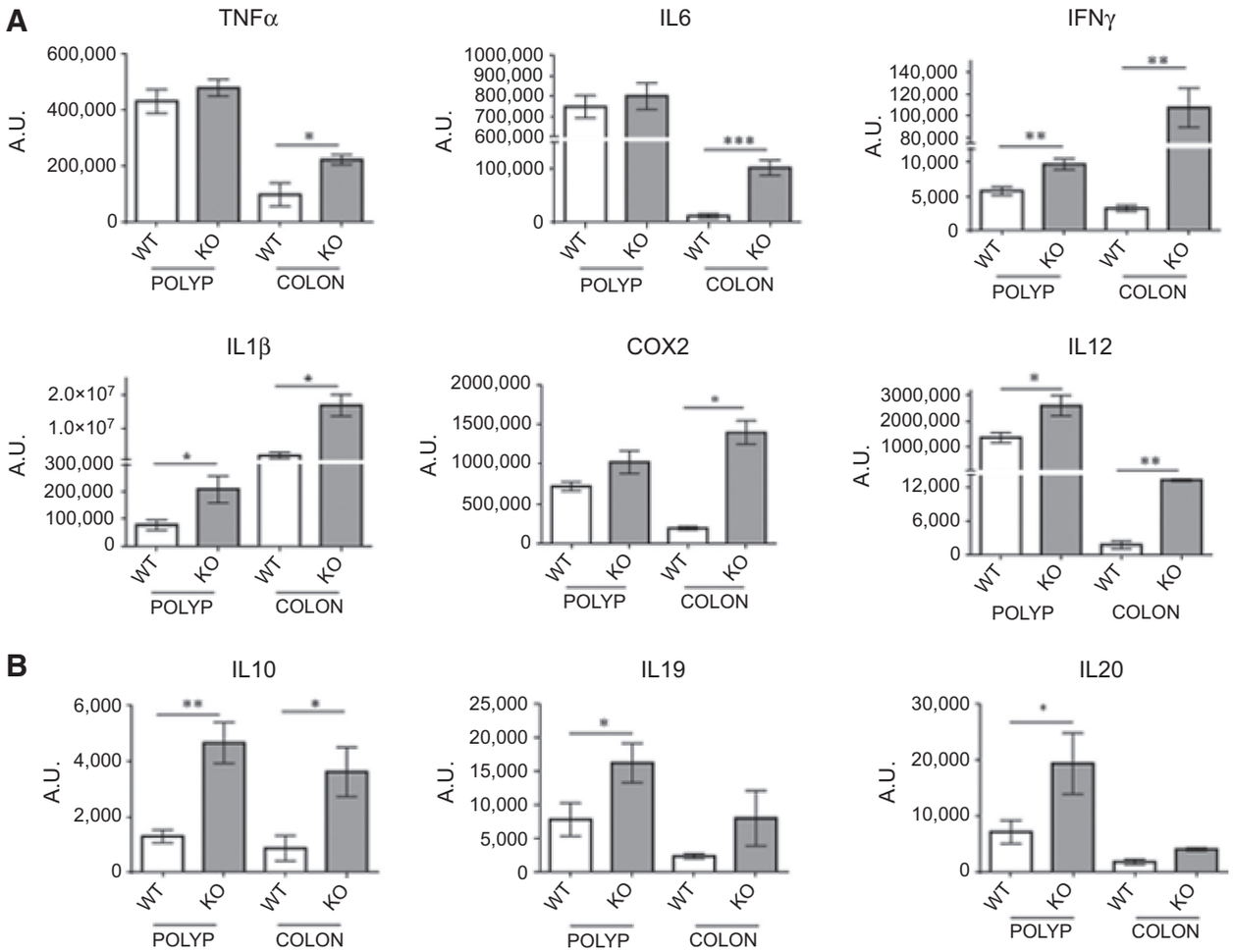

Figure 2.

mRNA expression of pro- and anti-inflammatory cytokines in the colonic tissue of CX3CR1$^{+/GFP}$ (WT) and CX3CR1$^{GFP/GFP}$ (KO) mice. Tumoral tissues (polyps) were separated from the rest of the colon and the two specimens were separately analyzed for the expression of different proinflammatory (**A**) or anti-inflammatory (**B**) cytokines. In KO mice, the expression of several proinflammatory mediators in the colons and polyps was higher than in WT mice. The IL10 family members (IL10, IL19, and IL20) were also upregulated in KO mice. Results are from one experiment with 8 mice per group, representative of five experiments performed with similar results. *t* test; *, $P < 0{,}05$; **, $P < 0{,}01$; ***, $P < 0{,}001$. A.U., arbitrary units.

macrophages (Fig. 1D). Inside the adenomatous polyps, macrophages were GFP^{Pos}, while at the border F4/80^{+} cells were mostly GFP^{Neg} (Fig. 1E), suggesting that, and in line with the literature, CX3CR1^{Hi} macrophages originate from CX3CR1^{Neg}-GFP^{Neg} newly recruited monocytes. The FACS analysis on disaggregated colons confirmed that more GFP^{+} macrophages were present in the gut of KO mice (Fig. 1F, left) and indicated that Ly6C^{Hi} inflammatory monocytes, but not Ly6C^{low} monocytes, were more abundant (Fig. 1F, middle and right).

We next evaluated the expression of inflammatory mediators. We dissected polyps from the inflamed colons and separately analysed the mRNA levels of proinflammatory and anti-inflammatory cytokines. As shown in Fig. 2A, the inflamed mucosa of KO mice contained higher levels of TNFα, IL6, IFNγ, IL1β, COX2, and IL12 (p35); IFNγ, IL1β, and IL12 were increased also in the adenomatous tissue. IL10 family members (IL10, IL19, and IL20) were also overexpressed in the gut of KO mice (Fig. 2B) and, importantly, the IL10R was not reduced (Supplementary Fig. S2A). As the homeostatic ability of CX3CR1 macrophages relies also on their response to IL10 (16), we verified that CX3CR1$^{GFP/GFP}$ macrophages were able to sense IL10. When stimulated *in vitro* with IL10, macrophages from KO mice correctly phosphorylated STAT3 as much as macrophages from WT mice (Supplementary Fig. S2B). Thus, the cytokine milieu of the colonic mucosa of CX3CR1-KO mice indicates an exacerbated inflammation, not attributable to a dysregulation of the IL10 system.

Inability of CX3CR1$^{GFP/GFP}$ mice to resolve acute inflammation

In view of the inability of KO mice to correctly control gut inflammation in the AOM/DSS model, we analyzed their behavior in the process of resolution from acute colitis. As shown in Fig. 3A, mice were treated with 1 cycle (7 days) of DSS followed by water for 3 or 6 days. By day 10, WT mice started to recover and at day 13 had completely recovered from colitis and were healthy, while KO mice still displayed severe signs of inflammation in terms of weight

Published OnlineFirst June 15, 2017; DOI: 10.1158/0008-5472.CAN-16-2501

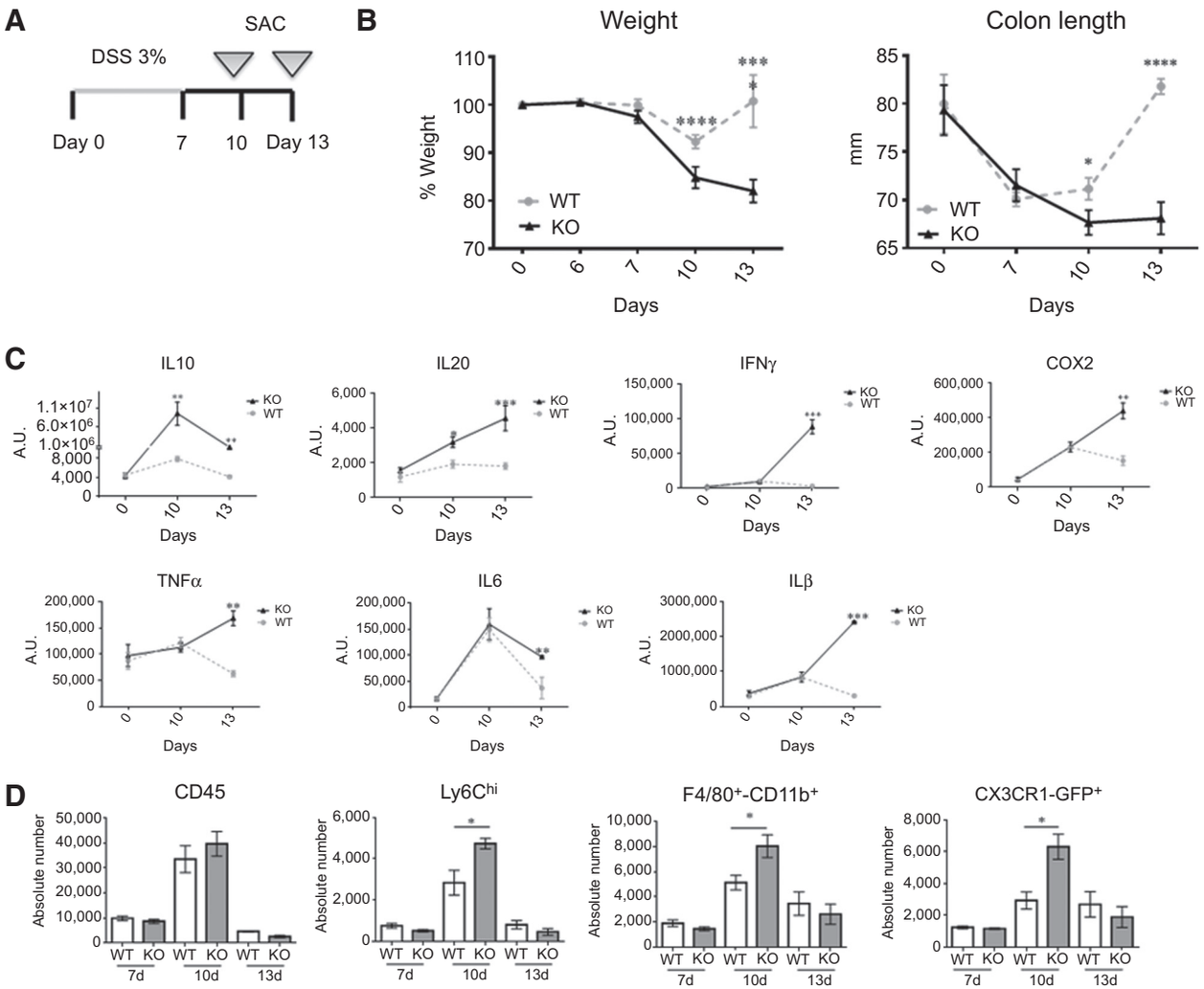

Figure 3.

CX3CR1$^{GFP/GFP}$ (KO) mice do not recover from acute colitis after DSS treatment. **A,** Treatment scheme of the DSS protocol. **B,** Body weight and colon length in WT mice were completely restored at day 13, but not in KO mice. **C,** Cytokine mRNA expression in the inflamed colonic tissues. IL10 and IL20 were higher in KO mice; proinflammatory cytokines were still upregulated at day 13 in KO mice, while they were decreased in recovering WT mice. A.U., arbitrary units. **D,** FACS analysis of colon samples revealed a peak of infiltrating leukocytes at day 10 with higher recruitment of macrophages (F4/80^{+} CD11b^{+} Ly6G^{-}) and inflammatory Ly6C^{hi} monocytes in KO mice Results are from one experiment performed with 4 mice per group for each time point, representative of five experiments performed with similar results. *t* test; *, $P < 0{,}05$; **, $P < 0{,}01$; ***, $P < 0{,}001$.

loss and colon shortness (Fig. 3B). The expression of inflammatory mediators was high at day 10 in both WT and KO mice, but at day 13 the mRNA levels of TNFα, IL6, IL1β, and COX2 were decreased in WT mice, while KO mice still showed sustained levels, in spite of significantly higher production of IL10 and IL20 (Fig. 3C). Colon tissues of KO mice had a more abundant infiltration of macrophages, especially GFP^{+} Mφ, and Ly6C^{Hi} inflammatory monocytes (Fig. 3D). Thus, KO mice are unable to successfully resolve inflammation in a prolonged model of colitis.

Intestinal carcinogenesis is more severe in the double knockout CX3CR1$^{GFP/GFP}$-APC^{Min} mice

To confirm that the absence of the CX3CR1 receptor in macrophages was associated to increased gut carcinogenesis, we crossed CX3CR1$^{GFP/GFP}$ mice with APC^{Min} mice, which carry a mutation in the APC gene, leading to the spontaneous development of polyps in the small intestine and, upon short DSS administration also in the colonic mucosa. Mice that were either competent or not for the expression of CX3CR1 and also carried the APC^{Min} gene were generated. As shown in the scheme of Fig. 4A, mice were administered DSS for one week and then water for four weeks. As observed in the previous sporadic model of CAC, double-KO mice (CX3CR1$^{GFP/GFP}$-APC^{Min}) showed higher signs of inflammation (higher DAI score and shorter colons) and a greater number of polyps compared with WT mice (CX3CR1$^{GFP/+}$-APC^{Min}; Fig. 4B and C). Furthermore, macrophages and proinflammatory monocytes were over-recruited in CX3CR1$^{GFP/GFP}$-APC^{Min} mice (Fig. 4D). The mRNA analysis of the colonic mucosa revealed the same results obtained in the AOM-DSS model: the

Published OnlineFirst June 15, 2017; DOI: 10.1158/0008-5472.CAN-16-2501

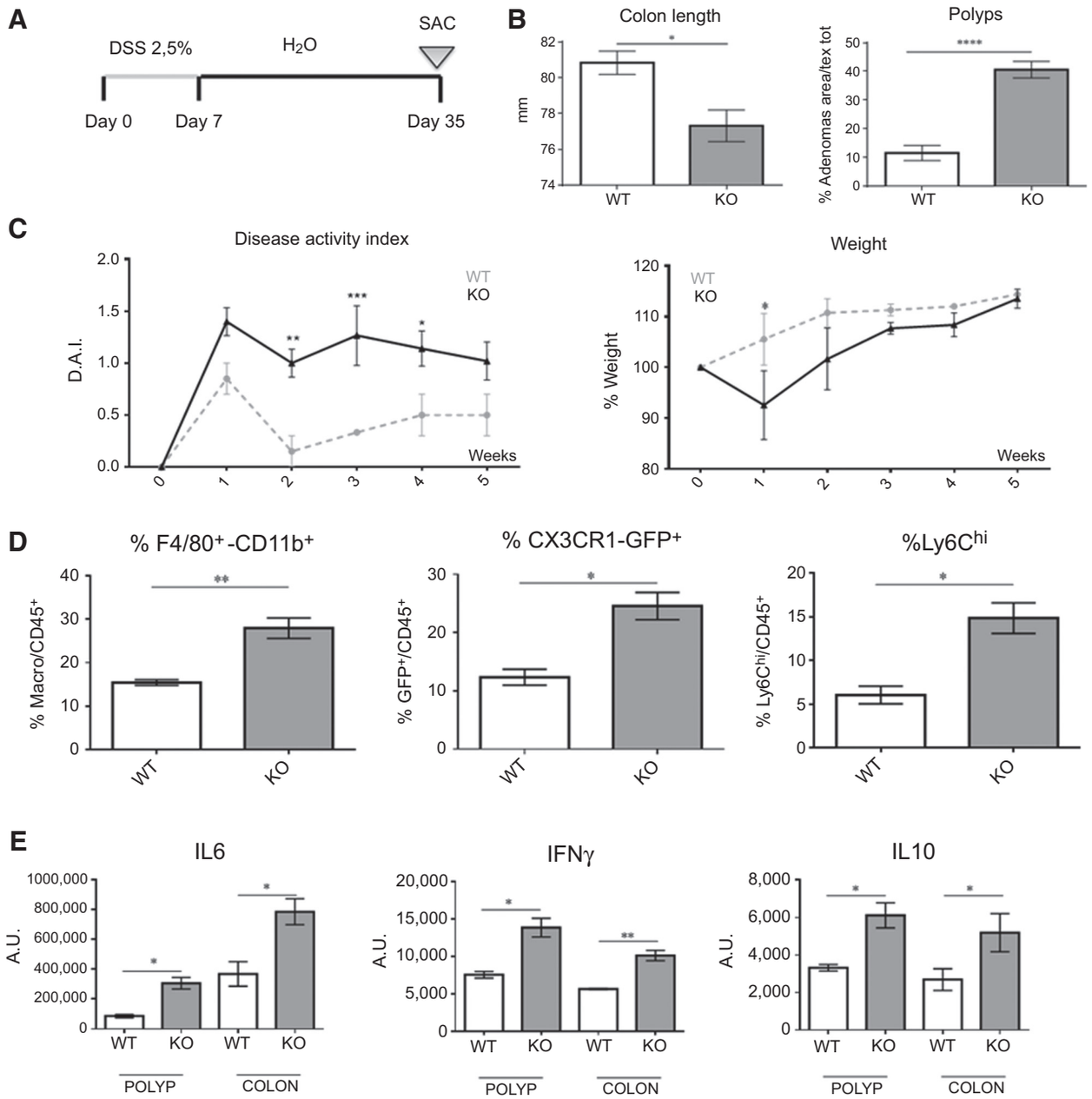

Figure 4.

Increased carcinogenesis and inflammation in DSS-treated APC^{min}- CX3CR1$^{GFP/GFP}$ mice. **A,** Treatment scheme of the DSS protocol in APC^{min} mice crossed with CX3CR1$^{GFP/GFP}$ mice. As it was for the AOM-DSS model, KO mice (APC^{min} -CX3CR1$^{GFP/GFP}$) showed higher signs of inflammation compared with WT mice (APC^{min} -CX3CR1$^{+/GFP}$). **B,** Colon length and number of polyps. **C,** Disease activity index and body weight. **D,** FACS analysis of disaggregated polyps. KO mice have higher infiltration of F4/80^{+} CD11b^{+} Ly6G^{-} macrophages, as well as of GFP^{+} macrophages and inflammatory Ly6C^{Hi} monocytes. **E,** Cytokine mRNA expression in the polyps and in colonic tissues. KO mice express higher levels of IL6, IFNγ, and IL10. In **B**, results are the mean of three experiments. Results in **C**–**E** are from one experiment with 5 mice per group, representative of three experiments performed with similar results; *t* test; *, $P < 0,05$; **, $P < 0,01$; ***, $P < 0,001$. A.U., arbitrary units.

inflammatory cytokines IL6, IFNγ, and IL10 were upregulated in KO mice in both polyps and colonic tissue (Fig. 4E). Overall, also in a genetic model of gut carcinogenesis, magnified by inflammation, KO mice are not able to properly control DSS-triggered colitis and this condition results in an aberrant inflammatory response and increased tumor formation.

The antioxidant enzyme HMOX-1 is directly induced by the CX3CL1–CX3CR1 axis

HMOX-1 is an enzyme known to have important antioxidant and anti-inflammatory activities (26–29). We explored the expression of HMOX-1 in the colon tissues of WT and KO mice. In all the animal models tested (AOM-DSS, CX3CR1$^{GFP/GFP}$

Published OnlineFirst June 15, 2017; DOI: 10.1158/0008-5472.CAN-16-2501

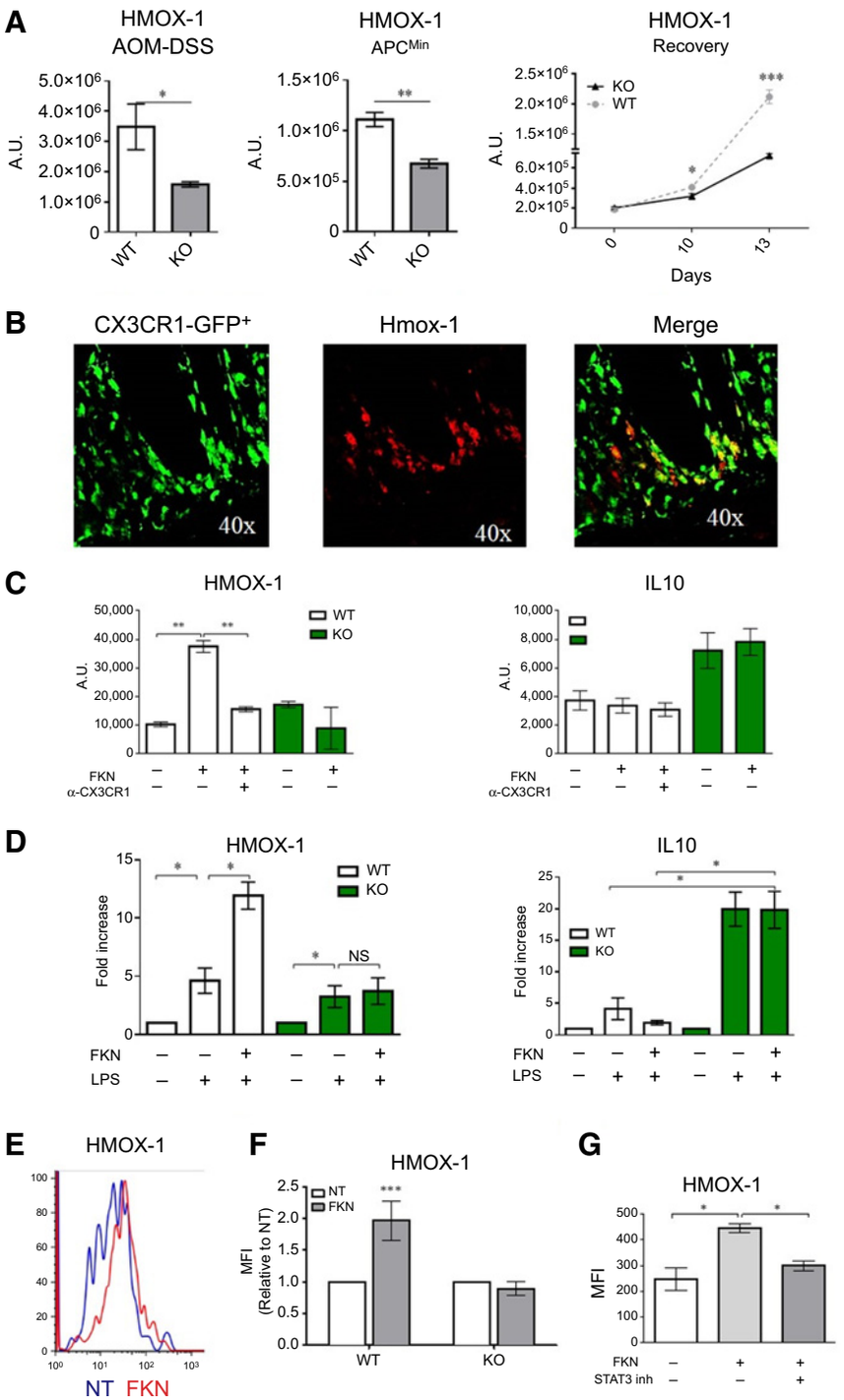

Figure 5.

CX3CR1 signaling induces heme-oxygenase-1 production. **A,** The mRNA expression of HMOX-1 is reduced in the adenomatous tissue of CX3CR1$^{GFP/GFP}$ KO mice, both in the AOM/DSS experiments, in the APC^{min} model, and in the inflamed tissue after the recovery from acute colitis. **B,** Immunofluorescence staining of HMOX-1 (red) in colonic tissue colocalizes with CX3CR1^{+} macrophages (GFP, green). **C,** Induction of HMOX-1 and IL10 upon *in vitro* treatment of GFP^{+}-sorted bone marrow-derived macrophages stimulated with rmCX3CL1 (300 ng/mL) and/or LPS (100 ng/mL); rmCX3CL1 activates HMOX-1 expression only in CX3CR1$^{+/GFP}$ WT mice. HMOX-1 was strongly inhibited by pretreatment with anti-CX3CR1 mAb in WT macrophages. A.U., arbitrary units. **D,** Low levels of HMOX-1 were induced by LPS in both WT and KO macrophages, but the strong synergism of combined rmCX3CL1 and LPS was observed only in CX3CR1-expressing WT mice. Instead, KO macrophages produced higher levels of IL10. NS, nonsignificant. **E,** FACS analysis of splenic CX3CR1$^{+/GFP}$ WT macrophages treated for 18 hours with 300 ng/mL of rmCX3CL1 and stained with anti-HMOX-1. CX3CL1 treatment (red line) increased HMOX-1 production. **F,** FACS analysis of HMOX-1 of gut macrophages from isolated lamina propria of WT or KO mice. Cells were treated with rmCX3CL1 as in **E**. Cells were gated as positive for CD45, CD11b, F4/80, and GFP. Results of HMOX-1 immunopositivity are expressed as fold (median fluorescence intensity, MFI) over untreated macrophages. **G,** FACS analysis with anti-HMOX-1 of splenic CX3CR1$^{+/GFP}$ WT macrophages treated for 18 hours with 300 ng/mL of rmCX3CL1. Pretreatment with the STAT3 inhibitor Stattic (1 μmol/L) inhibited HMOX-1 production. *t* test; *, $P < 0{,}05$; **, $P < 0{,}01$; ***, $P < 0{,}001$.

crossed with APC^{Min}, and recovery from acute colitis), HMOX-1 was significantly downregulated in KO mice (Fig. 5A). The immunofluorescence staining confirmed that CX3CR1-GFP^{+} cells are the main producers of HMOX-1 in the colonic mucosa (Fig. 5B).

We next investigated whether the ligand CX3CL1 was able to induce HMOX-1 production in macrophages. In bone marrow–derived macrophages, CX3CL1 significantly upregulated mRNA levels of HMOX-1 in WT macrophages from CX3CR1$^{+/GFP}$ mice, but no increase was detected in macrophages from KO mice (Fig. 5C). Pretreatment with a blocking anti-CX3CR1 Abs significantly reduced HMOX-1 expression, indicating a specific effect of the ligand (Fig. 5C). Similar results were found with concomitant stimulation of CX3CL1 and LPS that had a strong synergistic effect on HMOX-1 production in WT, but not in KO macrophages (Fig. 5D). On the other hand, CX3CL1 stimulation did not affect the production of IL10 (Fig. 5C and D). Notably,

Published OnlineFirst June 15, 2017; DOI: 10.1158/0008-5472.CAN-16-2501

macrophages from KO mice produced *in vitro* higher levels of IL10, a finding similar to what observed in the *in vivo* experiments (Fig. 5C and D).

We further confirmed that CX3CL1-treated macrophages from WT mice upregulated protein expression of HMOX-1 by flow cytometry in spleen macrophages (Fig. 5E), and in macrophages isolated from the colonic mucosa; this increase was not observed in macrophages from CX3CR1-deficient mice (Fig. 5F).

We further examined HMOX-1 production in macrophages and the potential link with signaling events downstream of the CX3CR1 receptor. Upon *in vitro* stimulation with the ligand CX3CL1, macrophages from WT mice showed early phosphorylation of STAT3, a finding previously unappreciated, but not of STAT1 (Supplementary Fig. S3); as expected, no phospho-STAT3 was detected in macrophages of KO mice (Supplementary Fig. S3). To corroborate this finding, we analyzed CX3CL1-induced HMOX-1 expression in WT macrophages pretreated with the STAT3 inhibitor Stattic (1 μmol/L). As shown in (Fig. 5G) HMOX-1 upregulation was reduced upon inhibition of STAT3 in macrophages.

Overall, the experiments demonstrated that HMOX-1 is regulated by the interaction of Fractalkine with its receptor CX3CR1, at least partially in a STAT3-dependent manner.

Microbiome influence in colitis-associated cancer

HMOX-1 is also involved in the clearance of bacteria in the intestinal lumen by increasing phagocytosis. Considering the lower levels of HMOX-1 in KO mice, we tested the *in vitro* phagocytic ability of macrophages from WT and KO mice. The percentage of LPS-coated beads internalized by KO macrophages was significantly lower than in control mice (Fig. 6A). We also found that the epithelial layer in the adenomatous tissue of KO mice showed a marked downregulation of the tight junction protein Zonula Occludens-1 (ZO-1; Fig. 6A), indicative of a damaged barrier. These findings prompted us to analyze the intestinal microbiota of mice treated with AOM-DSS, by 16S rRNA gene profiling of fecal metagenomic DNA at day 0 (steady state) and at sacrifice (day 70). To study α-diversity, Chao1 coefficient was used as predictor of taxonomic richness; in addition, the ecologic parameter of β-diversity was evaluated using Unifrac algorithms. As shown in Fig. 6B, at day 0 there were no differences in α-diversity between WT and KO mice. In contrast, after the treatment, WT mice displayed higher rate of Chao1 parameter compared with KO mice. This may be explained by the excessive immune response generated by higher inflammation, reducing bacterial richness. β-diversity analyses allow the comparison of the overall taxonomic microbiota composition among samples. We found that, differently from day 0, at sacrifice KO mouse samples clustered separately from WT in unweighted Unifrac plot (Fig. 6B), indicating that significant changes in the fecal microbiota composition originated between WT and KO mice throughout the DSS-induced inflammation and carcinogenesis process. The relative abundance of specific bacterial taxa was analyzed at the level of phylum, family, and genus in the two time points considered. At day 0 almost no differences were detectable between WT and KO; on the contrary, at sacrifice, three generations were markedly different between KO and WT samples: *Akkermansia*, *Lachnospira*, and *Bacteroides*. We tested the abundance of *Lachnospira* and *Bacteroides* by qPCR but, despite a tendency, no statistically significant differences between WT and KO mice were found (Supplementary Fig. S4A–S4C). On the contrary, qPCR experiments with primers targeting the species *Akkermansia muciniphila* evidenced a significant decrease of this bacterium in KO mice at sacrifice (Fig. 6B, right), while it was identically represented at day 0 in untreated WT and KO mice.

To test whether the intestinal microbiota can influence the microenvironment and has an impact on the CAC model, we cohoused WT and KO mice. Along the AOM-DSS experiment, weight and DAI score were registered every week, as represented in Fig. 6C (left). It was evident that the cohousing had a dramatic effect: both WT and KO cohoused mice displayed a lower DAI if compared with the classical AOM-DSS experiment (Supplementary Fig. S4A–S4C; Fig. 1B); furthermore, disease scores did not differ between WT and KO mice. The results clearly indicated that gut microbiota of the two strains was able to mutually influence each other and had an important effect on the disease. Indeed, *A. muciniphila* at the end of the experiment had similar mRNA levels in cohoused WT and KO mice (Fig. 6C, right). Nevertheless, some differences remained in terms of number of polyps, which were fewer than in the classical CAC model, bur still were significantly more in KO mice than in cohoused WT mice (Fig. 6C, middle).

To better understand how the cohousing decreased the severity of the disease, we extracted mRNA from polyps and determined the levels of both pro- and anti-inflammatory cytokines. As shown in Fig. 6D, the differences observed in the classical AOM-DSS model between WT and KO mice were no longer present and similar levels of TNF, IFNγ, and IL10 were detected. However, HMOX-1 still remained underexpressed in KO mice. Overall, the cohousing experiment resulted in an attenuation of the disease severity, lower inflammation, and higher capability to recover after DSS administration. In this landscape, only HMOX-1 was still lower and, indeed, colon carcinogenesis was only partially reduced by cohousing.

The pharmacologic upregulation of HMOX-1 protects from prolonged inflammation and colon carcinogenesis

On the basis of our results, the excessive mucosal inflammation found in KO mice could be ascribed to the reduced levels of HMOX-1 in mice lacking CX3CR1. To corroborate this finding, we pharmacologically modulated *in vivo* levels of HMOX-1 by treating mice with cobalt protoporphyrin IX (coPP), and inducer of HMOX-1, or with the inhibitor Zinc protoporphyrin (znPP). After administration of znPP, mice receiving 1 cycle of DSS showed a strong increase in the severity of the disease already at days 6, compared with vehicle-treated animals, and the disease index was still high at day 10, during the recovery phase (Supplementary Fig. S5). Conversely, the HMOX-1 inducer coPP completely ablated disease index, ulcer formation, and weight loss by day 9–10 (Supplementary Fig. S5). The phenotype of znPP-treated mice resulted so severe that it was not possible to go longer in time with the experiment. Therefore, the AOM-DSS experiment was performed with the HMOX-1 inducer coPP. Both $CXRCR1^{GFP/+}$ and $CX3CR1^{GFP/GFP}$ mice were treated with coPP four times a week during the DSS cycles, as detailed in the scheme in Fig. 7A. Strikingly, treatment with coPP was able to switch off inflammation also in KO mice compared with vehicle-treated mice: disease index scores were close to 0 and KO mice showed a recovery in weight similar to that of WT mice (Fig. 7B). At the end of the experiment (day 70), the histologic analyses revealed that the phenotype of coPP-treated KO mice was totally reverted with no signs of inflammation (Supplementary Fig. S6). Moreover, the

Published OnlineFirst June 15, 2017; DOI: 10.1158/0008-5472.CAN-16-2501

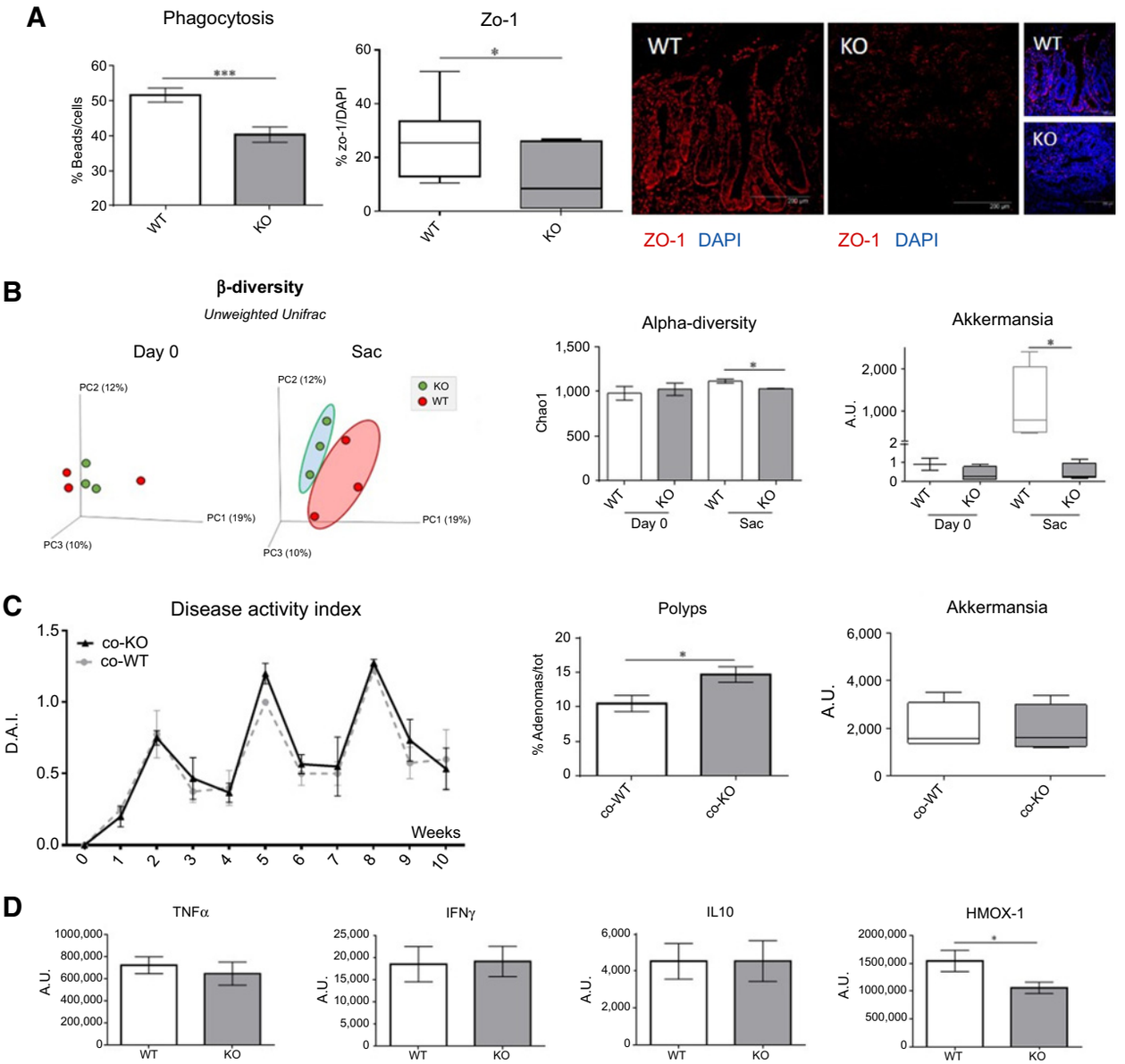

Figure 6.

Analysis of intestinal microbiota during AOM/DSS treatment and cohousing experiment of CX3CR1$^{+/GFP}$ (WT) and CX3CR1$^{GFP/GFP}$ (KO) mice. **A,** Phagocytosis of LPS-coated beads by peritoneal macrophages isolated from WT and KO mice. Immunofluorescence of the tight junction protein (ZO-1) in colons of AOM/DSS-treated mice. The mucosa of KO mice showd less ZO-1 protein expression, indicative of a damaged epithelial barrier. **B,** Bacterial profiling of the fecal microbiota of AOM/DSS-treated mice. Plots of α- and β-diversity in WT and KO mice were similar at day 0 but changed drastically at sacrifice (Sac). The bacterial genus *Akkermansia* was scarcely represented at day 0, but highly increased at sacrifice only in WT mice. **C,** AOM/DSS experiment in cohousing conditions of WT and KO mice. Disease activity index (D.A.I.) is identical in cohoused WT and KO mice and, at sacrifice, similar levels of *Akkermansia* were detected. Cohoused mice formed fewer polyps, nevertheless KO mice had significantly more polyps than WT mice. **D,** mRNA levels of pro- and anti-inflammatory cytokines in the colonic mucosa of cohoused mice were similar in WT and KO mice, but HMOX-1 was still lower in KO mice. Results are from one experiment with 8 mice per group, representative of two experiments performed with similar results. *t* test; *, $P < 0,05$; **, $P < 0,01$; ***, $P < 0,001$. A.U., arbitrary units.

formation of polyps was almost completely abolished by the treatment (Fig. 7C). Induction of HMOX-1 in the colon of treated mice was checked by Western blot analysis. In vehicle-treated animals, HMOX-1 protein was reduced in KO compared with WT mice, as mentioned above (Fig. 7D), but was significantly upregulated in coPP-treated animals, both in KO and WT mice, with similar levels. The high levels of inflammatory mediators found in KO mice were blunted upon coPP treatment, confirming the anti-inflammatory effect of HMOX-1 (Fig. 7E).

In conclusion, the pharmacological stimulation of HMOX-1 completely resolved the DSS-induced inflammation and protected mice from carcinogenesis.

Published OnlineFirst June 15, 2017; DOI: 10.1158/0008-5472.CAN-16-2501

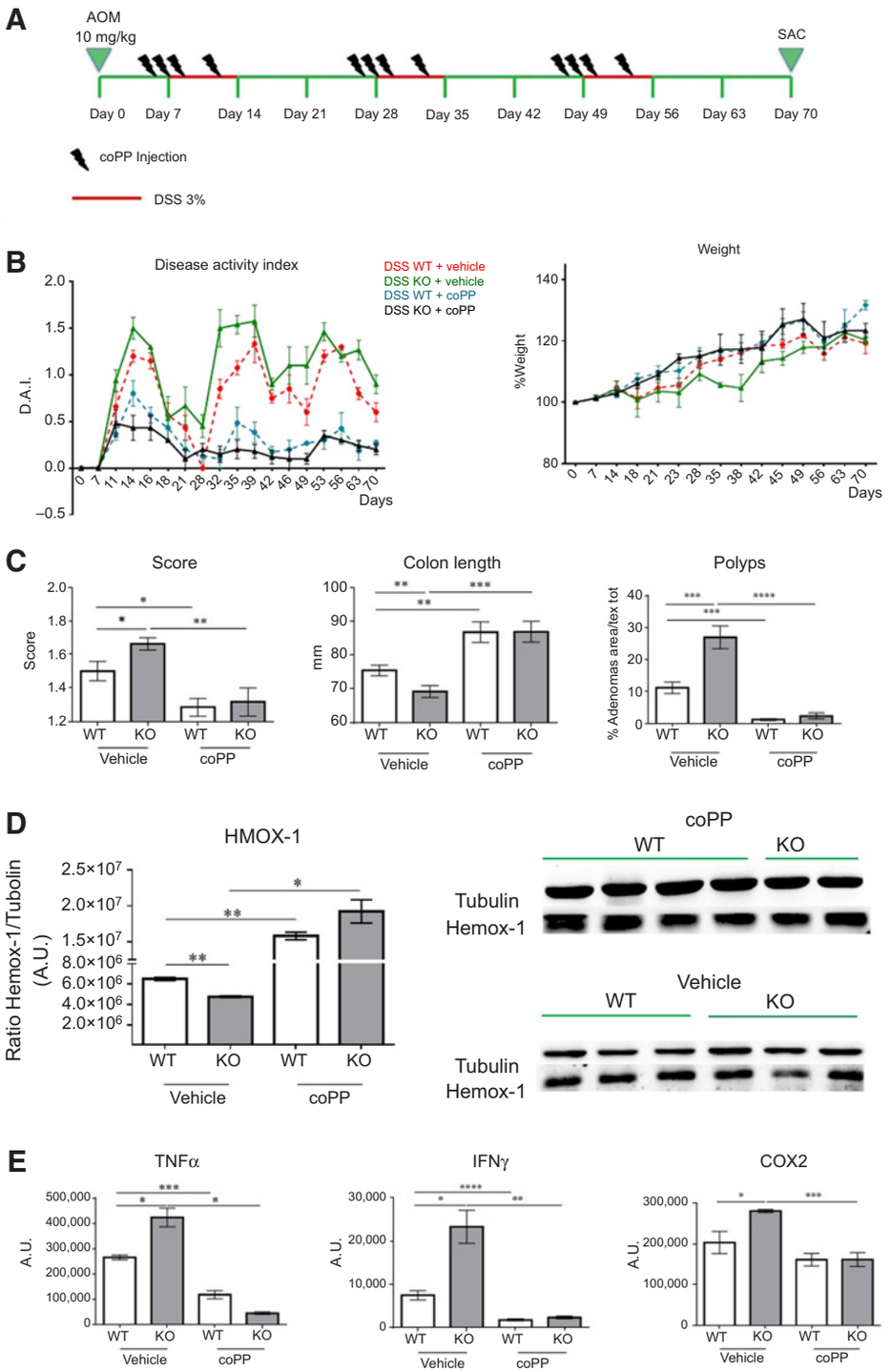

Figure 7.
Treatment with coPP increases HMOX-1 expression and ameliorates inflammation and carcinogenesis. **A,** Treatment scheme of coPP administration during the AOM/DSS protocol. **B** and **C**, In both WT and KO mice, coPP administration strongly reduces disease activity index (D.A.I.) and body weight (**B**), number of polyps, colitis score, and colon shortness (**C**). **D,** Western blot analysis to detect HMOX-1 in the colons of coPP-treated mice. Treatment increases HMOX-1 production in WT and KO mice. Vehicle-treated KO mice showed lower production of HMOX-1 compared with WT mice. **E,** mRNA expression of proinflammatory cytokines in colon tissue was higher in vehicle-treated KO mice, and strongly reduced upon treatment with coPP. Results are from one experiment, representative of three experiments performed with similar results. In **C**, results are the mean of three experiments. *t* test; *, $P < 0,05$; **, $P < 0,01$; ***, $P < 0,001$. A.U., arbitrary units.

Discussion

Chronic inflammation in the gut is strongly implicated in the promotion of carcinogenesis and disease progression (30–33). In this study, we show that CX3CR1-deficient mice were more susceptible in experimental models of intestinal carcinogenesis: colonic tissues were more infiltrated by inflammatory monocytes/macrophages and had higher levels of inflammatory cytokines. As a result of higher inflammation sustained over time, CX3CR1-KO mice had increased tumor load with significantly more adenomatous polyps. The exacerbated colonic inflammation in KO mice was not due to impaired IL10 production, which was actually increased compared with WT mice, or to defects of the IL10R, but to their inability to recover from inflammation.

Published OnlineFirst June 15, 2017; DOI: 10.1158/0008-5472.CAN-16-2501

Colon tissues of CX3CR1-KO mice had lower levels of HMOX-1, a crucial anti-inflammatory and antioxidant enzyme produced by macrophages and other cell types (34–36). HMOX-1 is the inducible form of the rate-limiting step of conversion of heme into carbon monoxide and biliverdin (37, 38). The well-known anti-inflammatory and tissue-protective effect of this enzyme was observed in patients affected by IBD and in mouse models of colitis (39–42). Upregulation of HMOX-1 results in a better outcome in experimental colitis and its protective effect is the result of radical scavenging (28, 43).

In vitro and *ex vivo* studies demonstrated that CX3CR1 engagement by its ligand CX3CL1/Fractalkine induced HMOX-1 upregulation in macrophages, via STAT3 phosphorylation. This induction was absent in CX3CR1-KO macrophages. HMOX-1 can be stimulated also by bacteria; the combination of LPS and CX3CL1 *in vitro* had a strong synergistic effect, but in KO mice HMOX-1 levels were dramatically lower. During DSS treatment, *in vivo* mice are exposed to a huge amount of endotoxin and other microbe-associated molecular patterns, due to disruption of the epithelial barrier and bacterial translocation. The finding that HMOX-1 levels in KO mice were lower, indicates that the CX3CL1–CX3CR1 axis is not redundant in the regulation of this enzyme in gut macrophages.

The CX3CR1 receptor in the colonic immune populations is largely expressed by macrophages (6, 44, 45), even though a very minor proportion of DC or activated T cells expressing low levels of CX3CR1 has been reported (12, 46, 47). Nevertheless, in the adenomatous polyps, our results clearly demonstrate that CX3CR1 is expressed by virtually all F4/80$^+$ macrophages, and not by CD103$^+$ DC or CD3$^+$ T cells (Supplementary Fig. S7).

Therefore, at least in the context of colon carcinogenesis, the CX3CL1–CX3CR1 axis impacts predominantly on gut macrophages for the induction of HMOX-1.

Other factors upregulating HMOX-1 include: heavy metals, hypoxia, thermal shock, free radical, heme, NO, and IL10 (48). Many studies suggested a synergism between IL10 and the microbiome in the induction of HMOX-1 (34, 49). It seems that the microbiota and its products stimulate HMOX-1 production via IL10, and the consequent CO formation facilitates bacteria clearance by macrophages (50). Lee and colleagues (48), demonstrated that the upregulation of HMOX-1 is dose-dependently induced by IL10. In our study, although IL10 levels were much higher in KO mice, this could not compensate the low expression of HMOX-1.

The phagocytic ability of KO macrophages was also impaired compared with CX3CR1-expressing cells of WT animals, in line with a previous report (51). Furthermore, we observed a profound alteration of the epithelial barrier in KO mice with a marked downregulation of the tight junction marker Zo-1. Thus, loss of barrier integrity, coupled with impaired phagocytosis, facilitates microbial translocation in tissues, generating inflammation and tissue damage.

The analysis of the bacterial taxonomic composition of the intestinal microbiota of mice treated with the AOM-DSS protocol indicated that, at steady state, no differences were detected between WT and KO mice. At the end of the experiment, KO mice had different bacterial composition, with reduced β-diversity, likely due to the exaggerated immune activation. These findings are in line with studies in human IBD, where the richness in bacterial species and their diversity is reduced during active disease, and also the stability in the composition of microbiota is changed (52, 53). The metagenomics analyses unveiled that at sacrifice a significant difference was found only for *Akkermansia*. *Akkermansia* is a bacterial genus that belongs to the Gram-negative phylum Verrucomicrobia and ascribes so far the only species *A. muciniphila*. Reportedly, *A. muciniphila* is able to efficiently degrade intestinal mucins and adhere on colonic epithelial cells, where it may promote the integrity of the epithelial cell layer (54). Notably, *A. muciniphila*, which is severely impaired during inflammatory bowel diseases, was demonstrated to reduce macrophage infiltration, downregulate proinflammatory chemokine expression, and attenuate metabolic endotoxemia in mice with Western diet–induced inflammation (55). Particularly, the reduction in circulating endotoxin level mediated by *A. muciniphila* was attributed to the induction of intestinal expression of tight junction proteins (55). These data are in agreement with the results of our study showing higher inflammation and altered intestinal barrier together with *Akkermansia* depletion in CX3CR1-KO mice. Moreover, being the mucus the native habitat of many species of bacteria, its alteration results also in a dysregulation of the total microbiome composition (56, 57). Therefore, the dysregulation observed in KO mice may be the consequence of their inability to produce sufficient amounts of HMOX-1 and to properly regulate the commensal microbiome and intestinal inflammation.

We analyzed whether the microbiome of WT mice was able to positively influence disease behavior of CX3CR1 KO mice. The results obtained with the cohousing experiment clearly indicated that the mixed composition of WT and KO microbiome had a positive effect in limiting tumor development, and all the histologic and inflammatory parameters were drastically ameliorated in KO mice. Importantly, the quantification of *Akkermansia* in fecal samples revealed the presence of this microorganism also in KO cohoused mice (but not in KO mice housed alone), underlying the beneficial role of this bacterium in the prevention of gut inflammation. Nevertheless, a significant difference in HMOX-1 production was still observed in cohoused KO mice, and more polyps were generated. This finding indicates that, in spite of the relevance of the microbiota, a functional CX3CL1–CX3CR1 axis is necessary to produce enough HMOX-1 to control inflammation in the intestine. That this enzyme has a crucial role in the protection from tumor development was fully confirmed in experiments where the pharmacologic induction of HMOX-1, by *in vivo* treatment with coPP, eradicated intestinal inflammation and protected KO mice from carcinogenesis. In conclusion, we have shown that HMOX-1 is produced downstream of the CX3CL1–CX3CR1 axis in gut macrophages. This pathway is nonredundant and necessary to control intestinal inflammation and to prevent the establishment of chronic colitis that leads to tumor development.

Disclosure of Potential Conflicts of Interest

No potential conflicts of interest were disclosed.

Authors' Contributions

Conception and design: G. Marelli, M. Erreni, P. Allavena
Development of methodology: G. Marelli, M. Erreni, P. Allavena
Acquisition of data (provided animals, acquired and managed patients, provided facilities, etc.): G. Marelli, M. Erreni
Analysis and interpretation of data (e.g., statistical analysis, biostatistics, computational analysis): G. Marelli, M. Erreni, V. Taverniti, S. Guglielmetti
Writing, review, and/or revision of the manuscript: G. Marelli, V. Taverniti, S. Guglielmetti
Administrative, technical, or material support (i.e., reporting or organizing data, constructing databases): S. Guglielmetti
Study supervision: A. Mantovani, P. Allavena
Other (flow cytometry experiment analysis): A. Anselmo

Acknowledgments

We thank Roberta Avigni for her help during the experiments.

Grant Support

P. Allavena received IG grants from the Italian Association for Cancer Research (AIRC). A. Mantovani received the grant 5 × 1000. M. Erreni was supported by a fellowship from Fondazione Umberto Veronesi.

The costs of publication of this article were defrayed in part by the payment of page charges. This article must therefore be hereby marked *advertisement* in accordance with 18 U.S.C. Section 1734 solely to indicate this fact.

Received September 14, 2016; revised February 1, 2017; accepted June 6, 2017; published OnlineFirst June 15, 2017.

References

1. Klose CS, Artis D. Innate lymphoid cells as regulators of immunity, inflammation and tissue homeostasis. Nat Immunol 2016;17:765–74.
2. Bain CC, Mowat AM. Macrophages in intestinal homeostasis and inflammation. Immunol Rev 2014;260:102–17.
3. Mowat AM, Agace WW. Regional specialization within the intestinal immune system. Nat Rev Immunol 2014;14:667–85.
4. Saleh M, Trinchieri G. Innate immune mechanisms of colitis and colitis-associated colorectal cancer. Nat Rev Immunol 2011;11:9–20.
5. Bain CC, Scott CL, Uronen-Hansson H, Gudjonsson S, Jansson O, Grip O, et al. Resident and pro-inflammatory macrophages in the colon represent alternative context-dependent fates of the same Ly6Chi monocyte precursors. Mucosal Immunol 2013;6:498–510.
6. Bain CC, Bravo-Blas A, Scott CL, Gomez Perdiguero E, Geissmann F, Henri S, et al. Constant replenishment from circulating monocytes maintains the macrophage pool in the intestine of adult mice. Nat Immunol 2014;15:929–37.
7. Ginhoux F, Schultze JL, Murray PJ, Ochando J, Biswas SK. New insights into the multidimensional concept of macrophage ontogeny, activation and function. Nat Immunol 2016;17:34–40.
8. D'Haese JG, Demir IE, Friess H, Ceyhan GO. Fractalkine/CX3CR1: why a single chemokine-receptor duo bears a major and unique therapeutic potential. Expert Opin Ther Targets 2010;14:207–19.
9. Varol C, Vallon-Eberhard A, Elinav E, Aychek T, Shapira Y, Luche H, et al. Intestinal lamina propria dendritic cell subsets have different origin and functions. Immunity 2009;31:502–12.
10. Niess JH, Brand S, Gu X, Landsman L, Jung S, McCormick BA, et al. CX3CR1-mediated dendritic cell access to the intestinal lumen and bacterial clearance. Science 2005;307:254–8.
11. Rimoldi M, Chieppa M, Larghi P, Vulcano M, Allavena P, Rescigno M. Monocyte-derived dendritic cells activated by bacteria or by bacteria-stimulated epithelial cells are functionally different. Blood 2005;106:2818–26.
12. Mazzini E, Massimiliano L, Penna G, Rescigno M. Oral tolerance can be established via gap junction transfer of fed antigens from CX3CR1(+) macrophages to CD103(+) dendritic cells. Immunity 2014;40:248–61.
13. Chieppa M, Rescigno M, Huang AY, Germain RN. Dynamic imaging of dendritic cell extension into the small bowel lumen in response to epithelial cell TLR engagement. J Exp Med 2006;203:2841–52.
14. Diehl GE, Longman RS, Zhang JX, Breart B, Galan C, Cuesta A, et al. Microbiota restricts trafficking of bacteria to mesenteric lymph nodes by CX(3)CR1(hi) cells. Nature 2013;494:116–20.
15. Esterhazy D, Loschko J, London M, Jove V, Oliveira TY, Mucida D. Classical dendritic cells are required for dietary antigen-mediated induction of peripheral Treg cells and tolerance. Nat Immunol 2016;17:545–55.
16. Zigmond E, Bernshtein B, Friedlander G, Walker CR, Yona S, Kim KW, et al. Macrophage-restricted interleukin-10 receptor deficiency, but not IL-10 deficiency, causes severe spontaneous colitis. Immunity 2014;40:720–33.
17. Hadis U, Wahl B, Schulz O, Hardtke-Wolenski M, Schippers A, Wagner N, et al. Intestinal tolerance requires gut homing and expansion of FoxP3+ regulatory T cells in the lamina propria. Immunity 2011;34:237–46.
18. Jung S, Aliberti J, Graemmel P, Sunshine MJ, Kreutzberg GW, Sher A, et al. Analysis of fractalkine receptor CX(3)CR1 function by targeted deletion and green fluorescent protein reporter gene insertion. Mol Cell Biol 2000;20:4106–14.
19. Konstantinova NA, Buravkova LB, Manuilova ES, Arsen'eva EL, Grivennikov IA. [Clinostatting effects on neuronal differentiation of embryonic stem cells from mice strain R1]. Aviakosm Ekolog Med 2010;44:65–7.
20. Medina-Contreras O, Geem D, Laur O, Williams IR, Lira SA, Nusrat A, et al. CX3CR1 regulates intestinal macrophage homeostasis, bacterial translocation, and colitogenic Th17 responses in mice. J Clin Invest 2011;121:4787–95.
21. Kayama H, Ueda Y, Sawa Y, Jeon SG, Ma JS, Okumura R, et al. Intestinal CX3C chemokine receptor 1(high) (CX3CR1(high)) myeloid cells prevent T-cell-dependent colitis. Proc Natl Acad Sci U S A 2012;109:5010–5.
22. Rossini V, Zhurina D, Radulovic K, Manta C, Walther P, Riedel CU, et al. CX3CR1(+) cells facilitate the activation of CD4 T cells in the colonic lamina propria during antigen-driven colitis. Mucosal Immunol 2014;7:533–48.
23. Marelli G, Belgiovine C, Mantovani A, Erreni M, Allavena P. Non-redundant role of the chemokine receptor CX3CR1 in the anti-inflammatory function of gut macrophages. Immunobiology 2016;222:463–72.
24. Ferrario C, Taverniti V, Milani C, Fiore W, Laureati M, De Noni I, et al. Modulation of fecal Clostridiales bacteria and butyrate by probiotic intervention with Lactobacillus paracasei DG varies among healthy adults. J Nutr 2014;144:1787–96.
25. Caporaso JG, Kuczynski J, Stombaugh J, Bittinger K, Bushman FD, Costello EK, et al. QIIME allows analysis of high-throughput community sequencing data. Nat Methods 2010;7:335–6.
26. Negi G, Nakkina V, Kamble P, Sharma SS. Heme oxygenase-1, a novel target for the treatment of diabetic complications: focus on diabetic peripheral neuropathy. Pharmacol Res 2015;102:158–67.
27. Ryter SW, Choi AM. Targeting heme oxygenase-1 and carbon monoxide for therapeutic modulation of inflammation. Transl Res 2016;167:7–34.
28. Chang M, Xue J, Sharma V, Habtezion A. Protective role of hemeoxygenase-1 in gastrointestinal diseases. Cell Mol Life Sci 2015;72:1161–73.
29. Soares MP, Hamza I. Macrophages and iron metabolism. Immunity 2016;44:492–504.
30. Mantovani A, Allavena P, Sica A, Balkwill F. Cancer-related inflammation. Nature 2008;454:436–44.
31. Hanahan D, Weinberg RA. Hallmarks of cancer: the next generation. Cell 2011;144:646–74.
32. Marelli G, Allavena P, Erreni M. Tumor-associated macrophages, multitasking cells in the cancer landscape. Cancer Res Front 2015;1:149–61.
33. Erreni M, Mantovani A, Allavena P. Tumor-associated macrophages (TAM) and inflammation in colorectal cancer. Cancer Microenviron 2011;4:141–54.
34. Whittle BJ, Varga C. New light on the anti-colitic actions of therapeutic aminosalicylates: the role of heme oxygenase. Pharmacol Rep 2010;62:548–56.
35. Guo X, Shin VY, Cho CH. Modulation of heme oxygenase in tissue injury and its implication in protection against gastrointestinal diseases. Life Sci 2001;69:3113–9.
36. N IJ, Rijnierse A, de Wit N, Jonker-Termont D, Dekker J, Muller M, et al. Dietary haem stimulates epithelial cell turnover by downregulating feedback inhibitors of proliferation in murine colon. Gut 2012;61:1041–9.
37. Maines MD. The heme oxygenase system: update 2005. Antioxid Redox Signal 2005;7:1761–6.
38. Paine A, Eiz-Vesper B, Blasczyk R, Immenschuh S. Signaling to heme oxygenase-1 and its anti-inflammatory therapeutic potential. Biochem Pharmacol 2010;80:1895–903.
39. Takagi T, Naito Y, Mizushima K, Nukigi Y, Okada H, Suzuki T, et al. Increased intestinal expression of heme oxygenase-1 and its localization in patients with ulcerative colitis. J Gastroenterol Hepatol 2008;23 Suppl 2:S229–33.

40. Paul G, Bataille F, Obermeier F, Bock J, Klebl F, Strauch U, et al. Analysis of intestinal haem-oxygenase-1 (HO-1) in clinical and experimental colitis. Clin Exp Immunol 2005;140:547–55.
41. Inui M, Ishida Y, Kimura A, Kuninaka Y, Mukaida N, Kondo T. Protective roles of CX3CR1-mediated signals in toxin A-induced enteritis through the induction of heme oxygenase-1 expression. J Immunol 2011;186:423–31.
42. Cavicchi M, Gibbs L, Whittle BJ. Inhibition of inducible nitric oxide synthase in the human intestinal epithelial cell line, DLD-1, by the inducers of heme oxygenase 1, bismuth salts, heme, and nitric oxide donors. Gut 2000;47:771–8.
43. Berberat PO, YI AR, Yamashita K, Warny MM, Csizmadia E, Robson SC, et al. Heme oxygenase-1-generated biliverdin ameliorates experimental murine colitis. Inflamm Bowel Dis 2005;11:350–9.
44. Bain CC, Hawley CA, Garner H, Scott CL, Schridde A, Steers NJ, et al. Long-lived self-renewing bone marrow-derived macrophages displace embryo-derived cells to inhabit adult serous cavities. Nat Commun 2016;7: ncomms11852.
45. Scott CL, Henri S, Guilliams M. Mononuclear phagocytes of the intestine, the skin, and the lung. Immunol Rev 2014;262:9–24.
46. Varol C, Zigmond E, Jung S. Securing the immune tightrope: mononuclear phagocytes in the intestinal lamina propria. Nat Rev Immunol 2010;10:415–26.
47. Rivollier A, He J, Kole A, Valatas V, Kelsall BL. Inflammation switches the differentiation program of Ly6Chi monocytes from antiinflammatory macrophages to inflammatory dendritic cells in the colon. J Exp Med 2012;209:139–55.
48. Lee TS, Chau LY. Heme oxygenase-1 mediates the anti-inflammatory effect of interleukin-10 in mice. Nat Med 2002;8:240–6.
49. Onyiah JC, Sheikh SZ, Maharshak N, Otterbein LE, Plevy SE. Heme oxygenase-1 and carbon monoxide regulate intestinal homeostasis and mucosal immune responses to the enteric microbiota. Gut Microbes 2014;5:220–4.
50. Naito Y, Takagi T, Higashimura Y. Heme oxygenase-1 and anti-inflammatory M2 macrophages. Arch Biochem Biophys 2014;564:83–8.
51. Ishida Y, Gao JL, Murphy PM. Chemokine receptor CX3CR1 mediates skin wound healing by promoting macrophage and fibroblast accumulation and function. J Immunol 2008;180:569–79.
52. Conte MP, Schippa S, Zamboni I, Penta M, Chiarini F, Seganti L, et al. Gut-associated bacterial microbiota in paediatric patients with inflammatory bowel disease. Gut 2006;55:1760–7.
53. Pitt JM, Vetizou M, Waldschmitt N, Kroemer G, Chamaillard M, Boneca IG, et al. Fine-tuning cancer immunotherapy: optimizing the Gut microbiome. Cancer Res 2016;76:4602–7.
54. Reunanen J, Kainulainen V, Huuskonen L, Ottman N, Belzer C, Huhtinen H, et al. Akkermansia muciniphila adheres to enterocytes and strengthens the integrity of the epithelial cell layer. Appl Environ Microbiol 2015; 81:3655–62.
55. Li J, Lin S, Vanhoutte PM, Woo CW, Xu A. Akkermansia muciniphila protects against atherosclerosis by preventing metabolic endotoxemia-induced inflammation in Apoe−/− mice. Circulation 2016;133:2434–46.
56. Png CW, Linden SK, Gilshenan KS, Zoetendal EG, McSweeney CS, Sly LI, et al. Mucolytic bacteria with increased prevalence in IBD mucosa augment in vitro utilization of mucin by other bacteria. Am J Gastroenterol 2010;105:2420–8.
57. Berry D, Reinisch W. Intestinal microbiota: a source of novel biomarkers in inflammatory bowel diseases? Best Pract Res Clin Gastroenterol 2013;27:47–58.

Published OnlineFirst June 15, 2017; DOI: 10.1158/0008-5472.CAN-16-2501

Cancer Research
The Journal of Cancer Research (1916–1930) | The American Journal of Cancer (1931–1940)

AACR American Association for Cancer Research

Heme-oxygenase-1 Production by Intestinal CX3CR1^{+} Macrophages Helps to Resolve Inflammation and Prevents Carcinogenesis

Giulia Marelli, Marco Erreni, Achille Anselmo, et al.

Cancer Res 2017;77:4472-4485. Published OnlineFirst June 15, 2017.